NASA Technical Paper 3128

August 1991

The Interaction of Hydrogen With Metal Alloys

M. D. Danford
and J. W. Montano

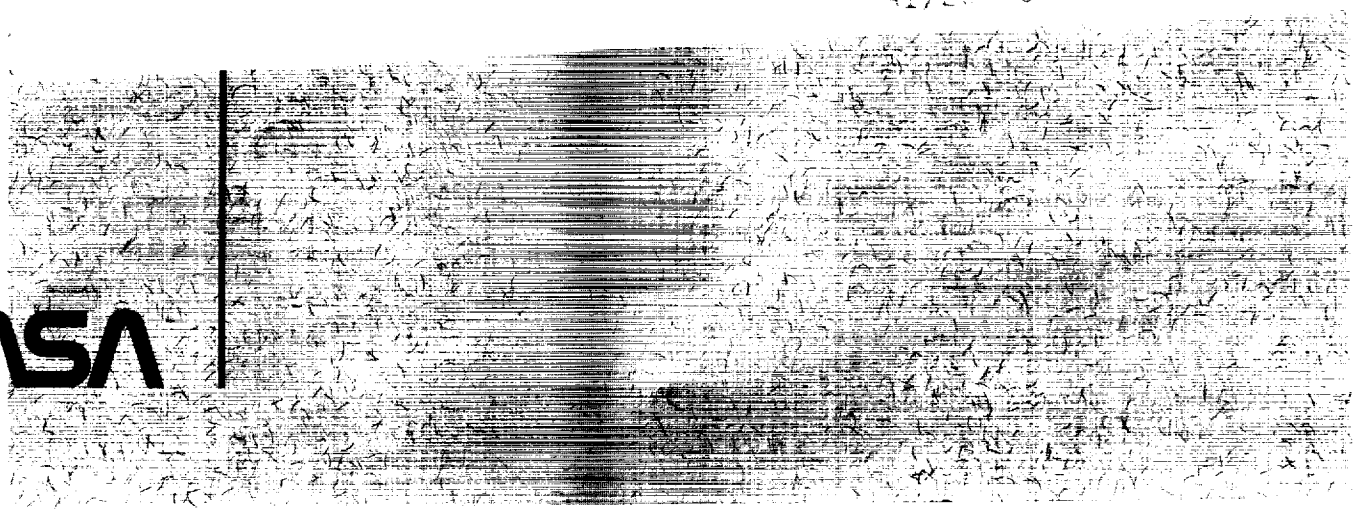

NASA

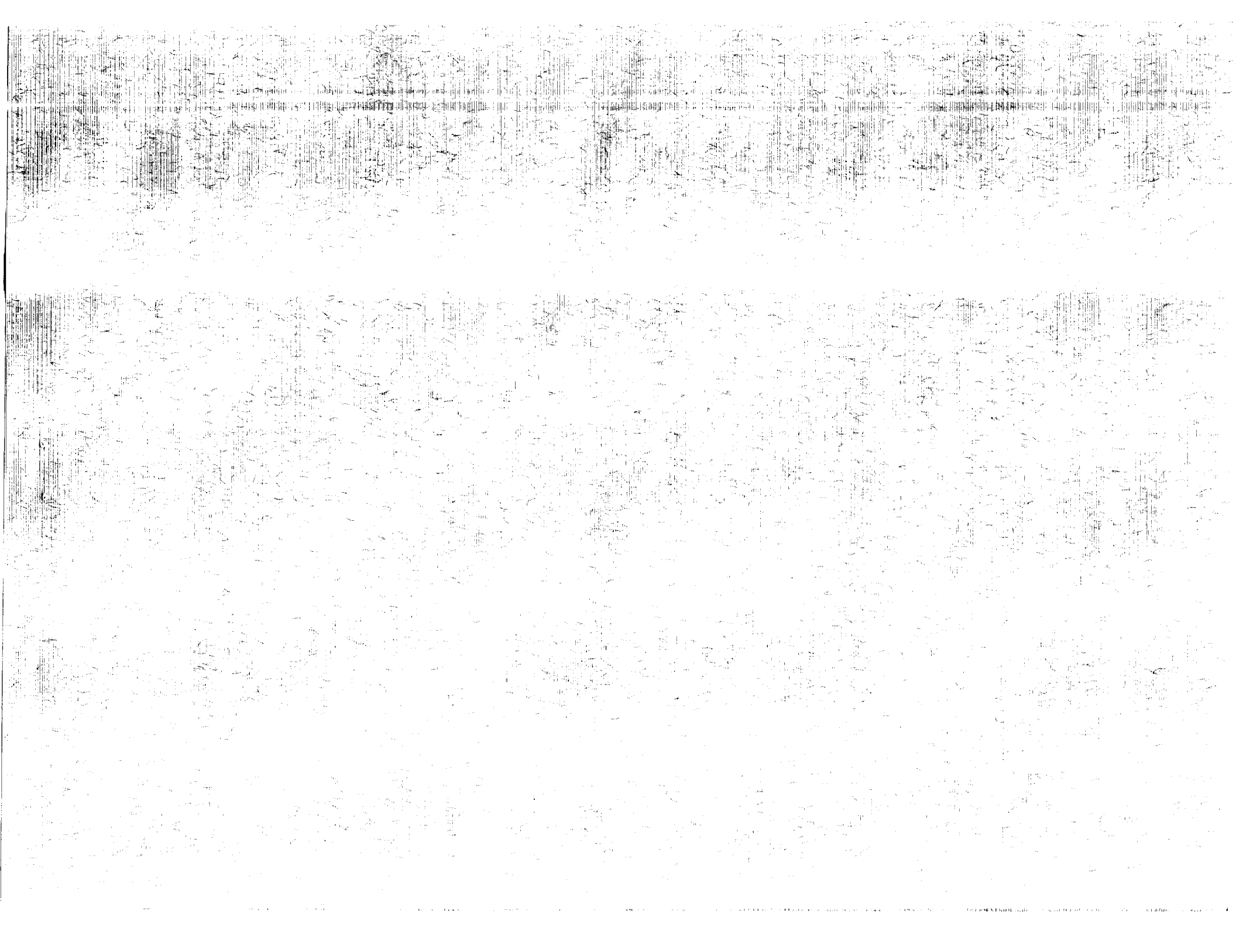

NASA Technical Paper 3128

1991

The Interaction of Hydrogen With Metal Alloys

M. D. Danford
and J. W. Montano
George C. Marshall Space Flight Center
Marshall Space Flight Center, Alabama

NASA
National Aeronautics and Space Administration
Office of Management
Scientific and Technical Information Program

TABLE OF CONTENTS

LIST OF ILLUSTRATIONS

LIST OF TABLES

CHEMICAL SYMBOLS

Al	aluminum
Co	cobalt
Cr	chromium
Fe	iron
Hg	hafnium
H_2SO_4	sulfuric acid
Mg	magnesium
Mo	molybdenum
$NaHSO_4.H_2O$	sodium bisulfate
Nb	niobium
Ni	nickel
Pd	palladium
Si	silicon
Ta	tantalum
Ti	titanium
TiC	titanium-carbide
V	vanadium
Zr	zirconium

TECHNICAL PAPER

THE INTERACTION OF HYDROGEN WITH METAL ALLOYS

INTRODUCTION

The interaction of hydrogen with the elemental metals, or components, of the alloys used in the space shuttle main engines (SSME), has been reported [1]. It was concluded in that report that metal elements have differing hydrogen affinities, and that a great part of hydrogen trapping is the result of semistable hydride formation rather than being due to hydrogen retention in grain boundaries, etc. The study of metal alloys has been undertaken in order to further extend the results of the previous work. Such variables as metal composition, grain structures, crystallographic structures, uniformities of hydrogen distributions on electrolytic charging at 25 °C, percent trapped hydrogen, and the extent of hydrogen retention on baking at 232 °C have been studied for several alloys in the present work. The susceptibility of the different alloys to hydrogen embrittlement is measured mechanically by the ratios of the notched tensile strengths of the alloys, $R(H_2/He)$, in high pressure (34.5 MPa (5,000 psi)) hydrogen to those in high pressure (34.5 MPa (5,000 psi)) helium. An attempt has been made to relate the susceptibilities of the alloys to hydrogen embrittlement to the variables listed above.

Hydrogen diffusion coefficients at 25 °C have been obtained for several metal alloys. The findings of these results and their implications regarding initial hydrogen distributions (distributions immediately after charging), grain structures, and crystallographic structures are discussed.

EXPERIMENTAL

Mobile hydrogen concentrations were determined electrochemically using cylindrical samples 2.54-cm long with a radius of 0.3175 cm. Samples were drilled and tapped on one end to accept a 3-48 thread as required by the sample holder. Sample holders for both cylindrical and flat samples have been shown previously [1]. The EG&G-PARC model 350A corrosion measurement console was employed for all electrochemical measurements. Flat samples with a thickness of 0.16 cm and a diameter of 1.43 cm were employed for the determination of all diffusion coefficients, since the geometry of the samples is more nearly ideal for this purpose and should give rise to values more comparable to those by other methods. However, diffusion coefficients obtained with cylindrical samples are the effective quantities for these specimens and were used in the calculations for mobile hydrogen concentrations. Samples were electrolytically charged at 25 °C for 1 h in 0.1N sulfuric acid (H_2SO_4) (no cathode poison was used) at a current density of 40 mA/cm^2. Charging of samples at the same current density was carried out in a eutectic mixture of molten sodium bisulfate ($NaHSO_4.H_2O$) and potassium bisulfate ($KHSO_4$) for the same timeframe at 150 °C.

Sample blanks were run at a constant potential of +0.25V(NHE) in a 0.1N sodium hydroxide (NaOH) solution at 25 °C. The period of measurement was 150,000 s for cylindrical samples, with data

points being recorded every 500 s. Longer periods of measurement were used for flat samples, providing a more accurate determination of diffusion coefficients. Data for hydrogen containing samples were collected in the same manner, with currents due only to hydrogen being obtained by subtraction of the currents for blanks. After each experiment, the current versus time data were read to an IBM PC/AT computer. Methods for data reduction to obtain coulombs of hydrogen desorbed versus time and initial hydrogen distributions (including values for the mobile hydrogen concentrations) within the samples for both cylindrical [2] and flat samples [3] have been described. The computer program PDEONE [4,5] was used for all calculations.

Total hydrogen concentrations were determined using a Leco model RH2 hydrogen analyzer. Specimens with a radius of 0.3175 cm and a length of 1.27 cm (half that used for electrochemical measurements) were used for all alloys. All specimens were charged in the same manner as that for the electrochemical measurements and at the same current densities. Calibration of the Leco analyzer was accomplished with standard samples. Hydrogen concentrations for charged samples were obtained after subtraction of values obtained for uncharged specimens or blanks. Trapped-hydrogen concentrations were obtained by subtracting mobile-hydrogen concentrations from the total-hydrogen concentrations obtained with the Leco analyzer.

To determine hydride stability, baking tests were conducted at 232 °C in air. Samples were baked 3 h each at this temperature, after which the remaining hydrogen concentrations were determined using the Leco analyzer. Values of C_0, the initial hydrogen concentrations, were obtained for charged, unbaked samples. The half-lives for hydrogen loss at 232 °C were obtained using the assumption of first-order kinetics, wherein the rate of hydrogen loss is proportional to the remaining hydrogen concentration.

Lattice constants for several of the alloys were determined by x-ray diffraction. For the determination of lattice constants and structure, flat specimens approximately 1.4 cm in diameter and 0.16-cm thick (the same dimensions as used for determination of hydrogen diffusion coefficients) were polished on one face, and x-ray patterns were recorded. Peak positions were corrected with a silicon standard and the lattice parameters determined. For the multiphase alloys MP35N and MP159, the percent face-centered cubic structures (the alloys contain a mixture of hexagonal close-packed and face-centered cubic structures) were determined through comparison with standards containing known amounts of the face-centered cubic arrangement.

RESULTS AND DISCUSSION

Crystal Structures

The crystallographic structures of several alloys are listed in table I. Most of the nickel-base alloys have the face-centered cubic structure, while those with high iron content (4340 alloy steel and Ni(250) maraging steel) have the body-centered cubic arrangement. However, both multiphase alloys MP35N and MP159, cold drawn and hardened to a tensile strength of 1,792 MPa (260 ksi), show a mixture of the hexagonal close-packed structure and face-centered cubic structure. Values of lattice parameters for the hexagonal close-packed structures for each were calculated using the 002 and 112 Bragg reflections, which were clearly evident in the x-ray diffraction patterns. The values of the lattice parameters so obtained are very close to those for elemental cobalt ($a = 2.51$ Å and $c = 4.08$ Å), which also has the hexagonal close-packed structure. Both of these alloys are high in cobalt content. The soft,

annealed metals are face-centered cubic with the hexagonal close-packed platelets being formed as a result of the cold work. The thin platelets of the hexagonal close-packed structure, which vary from 20 Å to 3,000 Å in thickness on the (111) planes of the face-centered cubic matrix, have been observed under high magnification.

Diffusion Coefficients

Diffusion coefficients for several alloys, as obtained from electrochemical hydrogen desorption measurements at 25 °C, are listed in table 2. As seen from the results, diffusion coefficients are about the same for all metals including the single crystal Pratt and Whitney (P&W) 1480 alloy. In fact, the average value of all diffusion coefficients is 2.11×10^{-8} cm^2/s with a standard deviation of only 0.81×10^{-8} cm^2/s for all coefficients. These results strongly suggest that hydrogen desorption takes place mainly through the metal lattice rather than through grain boundaries (there are extensive differences in grain sizes for the different alloys). Also, the diffusion coefficients, as measured by hydrogen desorption, do not depend on the type of crystallographic structure.

Hydrogen Desorption Curves

Hydrogen desorption curves for cylindrical samples of multiphase alloys MP159 and MP35N, Inconel 718, and cold-worked Inconel 718, P&W 1480, MAR-M-246 (Hf) and A-286, electrolytically charged with hydrogen at 150 °C, are shown in figures 1 through 7. Here, the alloys all exhibit highly uniform distributions as would be expected from the temperature variation of the diffusion coefficients (the values of diffusion coefficients increase with temperature). Thus, these curves are all in accord with the expectations of diffusion theory, and no behavior characteristic of structure is noted.

Hydrogen desorption curves for the same alloys charged at 25 °C are shown in figures 8 through 14. All samples except multiphase alloy MP35N exhibit nearly ideal behavior in the sense that they represent nearly nonuniform hydrogen distributions immediately after charging. The observed hydrogen desorption curve agrees more closely with that for a nonuniform hydrogen distribution which would be expected at 25 °C using the diffusion coefficient obtained from the hydrogen desorption data. A uniform hydrogen distribution would result from a much larger apparent diffusion coefficient for hydrogen absorption, perhaps differing from the observed value by an order of magnitude or more. Perhaps permeability, which involves both diffusion coefficients and solubilities, would be a more fitting consideration here. This type of behavior is characteristic of face-centered cubic samples charged at 25 °C and implies that the diffusion coefficients for hydrogen absorption are equal to those observed in the desorption process. On the other hand, body-centered cubic and hexagonal close-packed structures exhibit more nearly uniform distributions [1,2,3], implying that the diffusion coefficients for hydrogen absorption are much larger than those observed for hydrogen desorption.

The roles of both grain size and structure type in these processes will be discussed later. As stated previously, hydrogen desorption seems to take place mainly by diffusion through the metal lattice. Both multiphase alloys MP35N and MP150 contain mixtures of the hexagonal close-packed and face-centered cubic arrangements, and, as a result, would be expected to exhibit a more nearly uniform initial hydrogen distribution. However, MP150 was found to be 60-percent hexagonal close-packed while MP35N was

lower in this structure content (40 percent), as shown in table 1. As figures 8 and 9 indicate, MP159 shows a 22.5-percent uniform distribution while MP35N shows a 55.2-percent uniform distribution. Thus, the expected trends are reversed. The reason for the reversal of expected trends in percent uniformity are not understood in terms of the crystallographic structure, but might possibly result from differences in the grain structure. MP159 exhibits more cold work than does MP35N, as figures 15 and 16 indicate, and a greater content of the hexagonal close-packed structure is present.

The Role of Hydride Formation in Hydrogen Embrittlement

It is common for most metallurgists to consider hydrides as segregated phases in the metal matrix, and, as such, are visible to the optical or to the scanning electron microscope. However, the entry of a single hydrogen atom into the interstices of a metal lattice constitutes a hydride in the chemical sense, and, as such, is subject to all due considerations concerning the nature of the chemical bond. The fact that hydrogen atoms are entering the interstices of the metal lattice has been established conclusively by neutron diffraction for palladium [6], nickel [7], and zirconium [8]. The similarity of titanium and zirconium hydrides has been shown by x-ray diffraction [9]. The structure of both zirconium and titanium metals change from the hexagonal close-packed to a fluorite arrangement (fig. 19) as hydrogen atoms enter interstitial positions in the lattice. Nickel and palladium hydrides form a sodium chloride type structure with hydrogen atoms in the octahedral vacancies in the lattice. Palladium hydrides are stable while nickel hydrides are not stable. Chemical bonding has been postulated to be covalent in these structures [1,2,8]. The nickel-base alloys all form the face-centered cubic or austenitic structure. Also, it has been proposed [2] that hydrogen atoms enter the face-centered positions in the body-centered cubic arrangement of martensitic structures. Thus, basic crystallographic structures of metals cannot be ignored in studies of hydrogen embrittlement.

Relation of Structure to Hydrogen Distribution on Charging

It has previously been postulated that the structural dependence of the hydrogen distribution in metals on charging was connected mainly with the openness of the crystallographic arrangement [10]. In the face-centered structure, there is one octahedral vacancy per metal atom. In the body-centered structure, there are 1.5 sites and 2 sites per metal atom in the hexagonal close-packed and fluorite structures. The initial hydrogen distribution on charging becomes more uniform on charging at 25 °C with an increasing number of lattice sites available. However, with reference to table 3, it is clear that there is also a direct correlation with the grain size of the metal matrix, the hydrogen distribution being more uniform in body-centered structures where the grain sizes are much smaller than those of the nickel base, face-centered cubic alloys. Therefore, the probability of which of these factors is more predominant is open to question.

It is known that factors such as heat treatment and cold working affect the tendency toward hydrogen embrittlement, and that these factors also affect the metal grain structure. Therefore, the grain structure obviously plays a role in the susceptibility of a metal to hydrogen embrittlement. It is logical to think of the grain structure as being an important factor in hydrogen penetration, with absorption into the metal lattice taking place more readily in those metals with a large surface/volume ratio in the particles making up the metal matrix, i.e., the grain size. The body-centered cubic structures with small grains are

known to be much more subject to hydrogen effects than are the face-centered metals, such as the nickel-base alloys. The effect of cold working on grain size is shown in figures 17 and 18 for Inconel 718. However, other factors, such as elemental metal distribution, also play a role, along with the presence of metal carbides.

The tendency toward hydrogen embrittlement may also be influenced by the energy of the crystal lattice after hydrogen entry. Assuming complete occupancy of the lattice vacancies by hydrogen and a completely ionic structure, the crystal lattice energies are –330, –719, and –879 kcal/gm-atom of metal for the face-centered cubic, body-centered cubic, and the fluorite structures, respectively. No Madelung constant is available for the hexagonal close-packed structure. Although the bonding in the metal hydrides has been postulated to be covalent [1,8,10], there is resonance of the electron pair bond among the various possible bond directions with the electrons spending more time at hydrogen atom positions because of their greater electronegativity. Therefore, the energy of the lattice is much lower than that indicated by calculations for an ionic lattice, but the relative trends of the lattice energies may be similar for covalent bonding.

The Correlation of Structure and Composition With Notched Tensile Strength

The ratio of the notched tensile strength in (34.5 MPa (5,000 psi)) hydrogen to that in (34.5 MPa (5,000 psi)) helium, R(H_2/He), can be used as a criterion to estimate the resistance of metal alloys to hydrogen effects. These values are tabulated for several alloys in table 3. Those metal elements which form stable or semistable hydrides and which are contained in the metal alloys are also listed. The order of hydrogen affinity is Ta>Ti>Nb>Hf>V>Cr. These elements have been postulated to do most of the hydrogen trapping in metal alloys through hydride formation as hydrogen enters the metal lattice [1]. Along with these quantities, the relative grain sizes, percent uniformity of the initial hydrogen distribution on electrolytic charging at 25 °C, the percent trapped hydrogen (as measured by charging at 150 °C), the half-lives for hydrogen elimination on baking for samples charged at 150 °C (assuming first order kinetics), and the total hydrogen uptake on charging at 25 °C are also listed.

The percent of trapped hydrogen was measured on samples charged at 150 °C because the amount of hydrogen absorbed by the metals on charging is greater than at 25 °C, and, as a result, hydrogen measurements are more accurate. As discussed previously, there is a distinct correlation between grain size and percent uniformity of the initial hydrogen distribution on charging at 25 °C although there may be other reasons for this occurrence.

All metal alloys except 4340 (AMS 6414) and 18Ni(250) maraging steel trap hydrogen extensively. All of the alloys which trap hydrogen have large amounts of Cr, and many also have small quantities of Hf, V, Nb, Ta, or Ti. Tantalum has been determined to have the highest affinity for hydrogen of any of the metallic elements [11,12]. The observed half-life for hydrogen elimination (1.4 h) for the P&W 1480 alloys, shown in table 3, does not reflect this determination, but the percent trapping for this alloy is the highest of all the alloys studied. However, results of Vesely, Jacobs, and Verma [13], who studied the effects of high-pressure, high-temperature charging and baking of A-286, Inconel 718 and P&W 1480 alloys, indicate that the hydrogen retention is very high on baking P&W 1480, as compared to retentions by A-286 and Inconel 718. In that study, much higher hydrogen concentrations were involved, leading to more definitive results. Elemental tantalum metal has not been studied in this laboratory because of its high melting point (2,996 °C).

The half-life for hydrogen elimination on baking is of particular interest in relation to metal composition and $R(H_2/He)$ values. However, differences in hydrogen elimination half-lives for the metal alloys are not as strikingly different as are those from the pure metal elements [1] due to the small percentage of elements which form stable or semistable hydrides. Generally, alloys which contain elements forming the more stable hydrides have half-lives greater than 1 h in length. Inconel 718, both solution-treated and aged, and the solution-treated, cold-worked and aged, exhibits the largest half-life. This alloy contains a rather large amount of Nb + Ti, elements which form very stable hydrides. The difference between the half-life for conventionally heat-treated Inconel 718 (6.5 h) and that for the cold-worked Inconel 718 (4.5 h) is not considered significant. Conventional Inconel 718 exhibits a great deal of nonhomogeneity in grain sizes as well as irregular grain shapes which may be important factors in its poor hydrogen resistance. The percent uniformity for cold-worked Inconel 718 (19.0 percent) is almost twice as great as that for conventional Inconel 718 (11.4 percent) providing further evidence that smaller size grains are a factor in greater hydrogen permeability on charging. The value $R(H_2/He)$ for cold-worked Inconel 718 is 0.64 when measured at the normal load rate of 100,000 lb/min/in^2. This is to be compared to a value of 0.46 for conventional Inconel 718, the only difference being a much smaller grain size in the cold-worked specimen. Thus, for a given metal composition, smaller grain sizes lead to a greater hydrogen resistance.

Creating somewhat of a dilemma are Rene' 41 and Waspaloy. Although these metals are of very similar composition, the value of $R(H_2/He)$ is much better for Waspaloy (0.78) than it is for Rene' 41 (0.27). The apparent average grain size for Rene' 41 is smaller than that for Waspaloy, at least in the present determinations. Marked differences occur in the grain boundaries and in the distributions of carbides and other particles in the metal matrices. Rene' 41 exhibits a granular appearance in the grain boundaries which are noncontinuous and are composed of single rows of small white particles. As a result, the effective grain size is greatly increased. The composition of the grain boundary particles is given in table 4. Also, large dark carbide particles, some as large as 10 microns, are dispersed randomly throughout the metal matrix as well as are other white particles of about 13-microns diameter, which may represent a separate phase. The compositions of these particles are also listed in table 4.

Waspaloy, on the other hand, exhibits a conventional grain boundary structure in which the grain boundaries are sharply defined. Large carbides with diameters as great as 14 microns are present in the metal matrix, as are smaller, more numerous carbides of about 4-microns diameter. Fine particles with a diameter of about 1 micron are yet more numerous and are scattered throughout the metal matrix. The compositions of all particles are listed in table 5 for Waspaloy. Thus, the broader distribution of titanium in Waspaloy is probably beneficial to its greater hydrogen resistance, Ti and TiC both having high hydrogen affinities. Titanium is concentrated mostly in large carbides in the case of Rene' 41, and its distribution is less random. Another factor which may contribute to the poor hydrogen resistance of Rene' 41 is its granular and poorly defined grain boundary structure which probably results in a very large effective average grain size.

Values of $R(H_2/He)$ were not available for 4340 (AMS 6414) and 4340M. Presumably, the value of $R(H_2/He)$ for 4340 (AMS 6414) is very low, but a significant improvement in hydrogen resistance for 4340M has been reported [14]. The increased hydrogen trapping and hydrogen resistance of 4340M is believed due to the presence of vanadium. Elemental vanadium has been shown to exhibit very great hydrogen uptake on charging at 25 °C, with the stability of the resulting hydride being intermediate in nature, similar to that of chromium [1].

The multiphase alloys MP35N and MP159 are of particular interest. In this study, the alloys have been solution treated, cold worked, and aged to the same strength level (1,792 MPa = 260 ksi). The alloys are somewhat similar in composition except that MP159 also contains iron, titanium, and niobium, together with a small amount of aluminum. The compositions of MP35N and MP159 are tabulated in table 6. The major difference, as far as hydrogen trapping elements are concerned, lies in the small amounts of titanium and niobium contained in MP159. The half-life for hydrogen elimination is 1.3 h for MP35N and 3.1 h for MP159, probably within the experimental error associated with the measurement. However, the penetration of hydrogen into MP35N on charging at 25 °C is much greater than that for MP159, as indicated by the observed percent uniformity of the hydrogen distribution. The value observed for MP35N is comparable to those observed for the body-centered cubic metals listed in table 3, which all exhibit poor hydrogen resistance. Values of $R(H_2/He)$ are 0.64 and 0.82 for MP35N and MP159, respectively. The increased hydrogen resistance of MP159 is believed due not only to the lower penetration of hydrogen, but also to the presence of the stable hydride formers Nb and Ti, which increase the hydrogen trapping ability of the metal. The (0.82) $R(H_2/He)$ of MP159 alloy (1,792 MPa (260 ksi) UTS) is the highest of any of the high-strength alloys tested in this program.

Incoloy 903, which demonstrates the highest resistance to hydrogen effects of any of the alloys, contains almost equal amounts of Cr, Nb, Ti, and Ta. In addition, the metal matrix is interspersed with intragranular carbides of Ti and Ti plus Nb. These have been characterized as larger occupancy, irreversible trap sites for hydrogen (high energy traps) [15] and are believed to be responsible in large part for the hydrogen resistance of Incoloy 903.

CONCLUSIONS

Hydrogen diffusion coefficients have been determined to be about the same at 25 °C for all alloys included in this work. Diffusion in hydrogen desorption is believed to take place through the metal lattice, whereas diffusion in the absorption process can take place in two ways, either through the metal lattice or initially through the grain boundaries with subsequent absorption into the metal lattice. The data correlate with either mechanism.

Hydrides are believed to play an important role in the hydrogen resistance of metal alloys. It is not meant to imply that hydrides must be present as observable phases in the metallurgical sense, but that they occur through the entry of hydrogen atoms into interstices of the metal lattice, forming hydrides in a chemical sense which are subject to all rules for chemical bonding. Varying degrees of hydride stability are observed, the order of stabilty for elemental metals being Ta>Ti>Nb>Hf>V>Cr. The presence of a small amount of any of these elements seems to be beneficial. Tantalum is very effective as a hydrogen trapping agent. Elemental Ta has not been studied in this laboratory because of its very high melting point. Vanadium and chromium, which form hydrides of intermediate stability, seem to play a positive role in increasing the hydrogen resistance of alloys. However, hydrogen resistance seems to depend not only on the presence of hydrogen trapping elements, but also on their distribution in the metal matrix. The presence of Ti and Ti plus Nb carbides seems to play a highly beneficial role in some cases. Titanium-carbon and niobium-carbon form high-energy, irreversible hydrogen traps which are capable of attracting rather large quantities of hydrogen. Very large, concentrated Ti and Nb containing particles seem to have a negative influence on hydrogen resistance while small, highly dispersed particles seem to have a positive influence.

Such factors as grain size also play a role. This is clearly demonstrated in the case of normal and cold-worked Inconel 718, where the very small grain size in the cold-worked specimen led to a greater hydrogen resistance. Grain shapes are also important. The necklace structure, which is characteristic of thermomechanically processed Waspaloy and is composed of very large grains surrounded by multiple granules, displays a decided improvement in hydrogen resistance [16]. A recent study [17] suggests that hydrogen embrittlement susceptibility is strongly linked to grain-boundary structures. Boundaries possessing large gaps and structural irregularities are adversely affected, while those lacking these defects are resistant to embrittlement.

Chromium is usually present in rather large amounts, whereas only small amounts of V are usually included in metal alloys. Vanadium is known to absorb copious amounts of hydrogen on charging at 25 °C, but unfortunately it is not a part of most of the nickel-base alloy compositions. It is suggested that a small amount of V be considered for inclusion in nickel-base alloys in order to determine its effect on hydrogen resistance. Along with this, the effect of V on the normal mechanical properties should be examined. Finally, it should be pointed out that metal alloys whose composition tends toward either pure iron or pure nickel, in the absence of trapping elements, generally show a smaller resistance to the effect of hydrogen. In either case, no hydrogen trapping occurs and hydrides are unstable, leading to an increasing mobile hydrogen content. Much basic work needs to be done to completely understand all conditions leading to the causes and corrections for hydrogen embrittlement in metals, and all metallurgical, chemical, and crystallographic aspects of the problem should be considered.

REFERENCES

1. Danford, M.D.: NASA Technical Paper 2882, January 1989.

2. Danford, M.D.: NASA Technical Paper 2744, July 1987.

3. Danford, M.D.: NASA Technical Memorandum TM-86531, October 1985.

4. Murphy, W.D.: Rockwell International Science Center Internal Report SC-DIT-76-10, 1976.

5. Sincovec, R.F., and Madsen, N.K.: ACM Trans. Math. Software, vol. 1, 1975, pp. 232–260.

6. Worsham, J.E., Wilkinson, M.K., and Shull, C.G.: J. Phys. Chem. Solids, vol. 3, 1957, p. 303.

7. Wollan, E.O., Cable, J.W., and Koehler, W.C.: J. Phys. Chem. Solids, vol. 12, 1959, p. 206.

8. Rundle, R.E., Shull, C.G., and Wollan, E.O.: Acta Cryst., vol. 5, 1952, p. 22.

9. Sof'ina, V.V., Azarkh, Z.M., and Orlova, N.N.: Crystallography of the Academy of Science of the USSR, vol. 3, No. 1, 1958, p. 544.

10. Danford, M.D.: NASA Technical Paper 2842, September 1988.

11. Wagner, C.: Thermodynamics of Alloys, Addison-Wesley, Reading, MA, 1952, p. 47.

12. Lupis, C.H.P., and Elliot, J.F.: Acta Met., vol. 15, 1967, p. 265.

13. Vesely, E.J., Jr., Jacobs, R.K., and Verma, S.K.: Report No. IITRI-P06150-P413, November 1990.

14. Raymond, L.: Contract DAAG 46-85-C-0020, MTL TR86-42, U.S. Army Materials Laboratory, October 1986.

15. Pressouyre, G.M., and Bernstein, I.M.: Metallurgical Trans., vol. 16A, 1985, p. 1879.

16. McPherson, W.B.: Private communication.

17. Smith, R.W., and Was, G.S.: Phys. Rev., vol. 40, No. 15, November 1989, p. 10 322.

Table 1. Structures of alloys.

Alloy	Structure	d, Å
347SS	FCC[1]	3.60
MP159	FCC(40%)+HCP	3.61(FCC)*
MP35N	FCC(60%)+HCP	3.60(FCC)**
Rene' 41	FCC	3.60
Waspaloy	FCC	3.58
Inconel 718(CW)	FCC	3.61
Inconel 718	FCC	3.60
Incoloy 903	FCC	3.60
A-286	FCC	3.60
4340 (AMS 6414)	BCC	2.87
4340M	BCC	2.87
Ni(250) Maraging Steel	BCC	2.87
440C	BCC	2.87

1 FCC = Face-centered Cubic, HCP = Hexagonal Close-packed, BCC = Body-centered Cubic

* Values obtained for a and c were 2.55Å and 4.08Å respectively for HCP structure.

** Values obtained for a and c were 2.54Å and 4.06Å respectively for HCP structure.

Table 2. Hydrogen diffusion coefficients at 25 °C.

Alloy	$D(cm^2/sec)x10^8$
347SS	1.16
MP159	2.53
MP35N	2.53
1480	2.94
Inconel 718(CW)*	3.78
Inconel 718	1.88
Incoloy 903	1.28
Waspaloy	2.15
Rene' 41	1.47
A-286	0.99
4340	2.29
MAR-M-246 (Hf)	2.26
440C	1.30

* CW = Cold Worked

Table 3. Comparison of properties for several alloys.

Alloy	H_2 Trapping Elements Hf	V	Cr	Nb	Ta	Ti	Grain Size Microns	% Uniformity 25°C	% Trapped H_2(150°C)	$t_{½}$ (Hours)	$R(H_2/He)$*	H_2 Uptake, 25°C ppm **
MAR-M-246	1.8	-	9.0	-	1.5	1.5	-	7.7	62.2	2.4	0.40(DS)	0.67
P&W 1480	-	-	10.0	-	12.0	1.5	-	22.4	91.8	1.4	0.57(100)[2]	1.30
Waspaloy	-	-	19.5	-	-	3.0	162	3.3	56.4	1.1	0.78	0.57
Incoloy 903	-	-	1.0	1.2	1.2	1.4	122	4.5	57.3	1.3	1.0	0.72
Inconel 718	-	-	19.0	5.1	-	0.9	58	11.4	81.5	6.5	0.46	0.38
Inconel 718(CW)	-	-	19.0	5.1	-	0.9	20	19.0	83.1	4.5	0.64	0.92
MP 35N	-	-	20.0	-	-	-	61	55.2	85.9	1.3	0.64	0.65
MP 159	-	-	19.0	0.6	-	3.0	67	22.5	83.3	3.1	0.82	0.52
347SS	-	.03	19.0	1.0	-	-	43	32.1	76.0	1.5	0.91	0.57
Rene' 41	-	-	19.1	-	-	3.2	66	0.0	86.5	3.2	0.27	1.11
A-286	-	0.3	15.0	-	-	2.0	71	0.0	73.7	1.3	0.97	0.33
4340 (6414)	-	-	0.8	-	-	-	27	50.7	0.0	-	-	0.81
4340M	-	0.1	0.8	-	-	-	8	82.5	48.0	1.9	-	1.01
18Ni(250)MS	-	-	-	-	-	0.4	19	63.0	0.0	-	0.12	0.96
440C	-	-	17.7	-	-	-	46	50.3	51.8	0.5	0.50	1.65

* 34.5 MPa (5000 psi) Pressure.

** Hydrogen uptake at 25°C, all alloys under same charging conditions.

1 DS = Directionally Solidified

2 Single crystal, value of $R(H_2/He)$ in (100) orientation. Value of $R(H_2/He)$ increases in other orientations.

Table 4. Comparison of structures particles in Rene' 41 (weight percent).

Element	White Particles	Large Dark Carbides	Grain Boundary Particles
Si	0.26	1.0	0.27
Ti	1.83	61.48	0.83
Cr	11.55	4.19	0.43
Co	9.46	-	10.69
Ni	59.21	-	72.92
Mo	17.69	33.32	5.34
Al	-	-	0.13
Fe	-	-	1.40

Table 5. Compositions of structural particles in Waspaloy (weight percent).

Element	Large Carbides	Small Carbides	Fine Particles
Si	-	-	-
Ti	75.14	58.33	3.48
Cr	1.26	3.29	6.73
Co	-	-	11.07
Ni	4.59	1.28	76.17
Mo	-	36.95	1.43
Al	12.0	-	0.14
Fe	0.25	0.06	0.97
Mg	6.76	-	-

Table 6. Compositions of multiphase alloys MP35N and MP159.

Alloy	Composition, Percent							
	Ni	Co	Cr	Fe	Mo	Ti	Nb	Al
MP35N	35.0	35.0	20.0	-	10.0	-	-	-
MP159	25.5	35.7	19.0	9.0	7.0	3.0	0.6	0.2

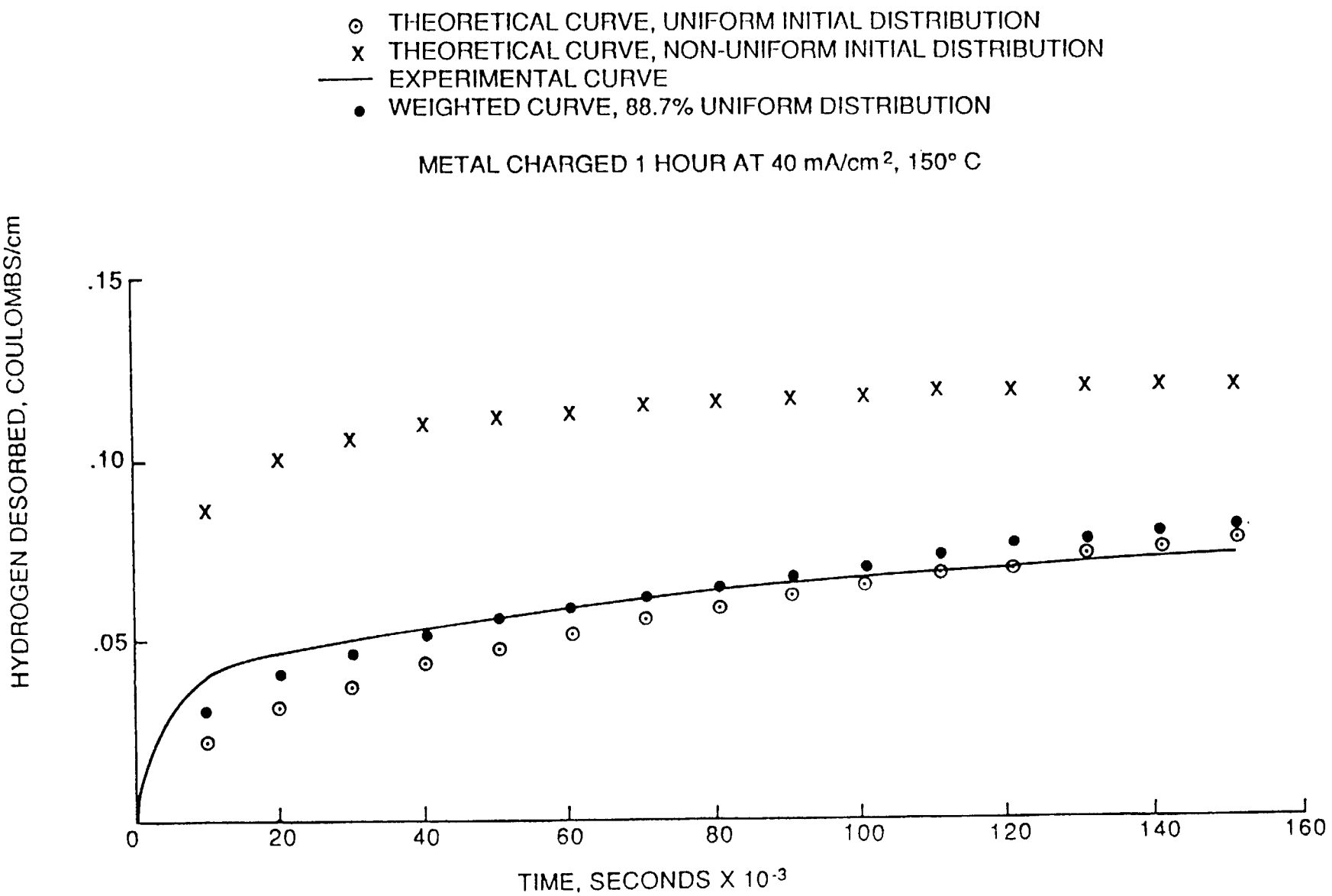

Figure 1. Hydrogen desorption curves for MP159 cylinder charged at 150 °C.

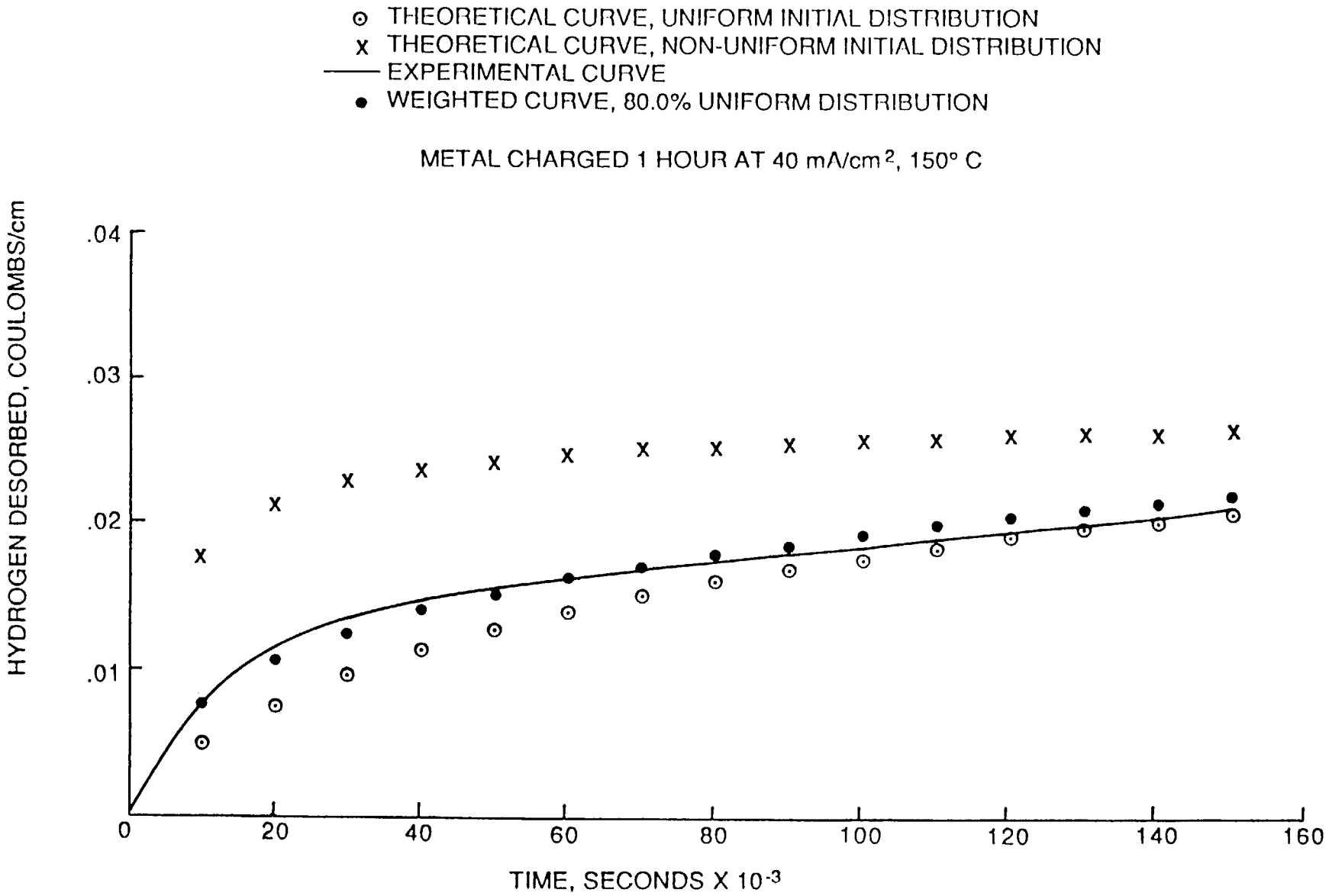

Figure 2. Hydrogen desorption curves for MP35N cylinder charged at 150 °C.

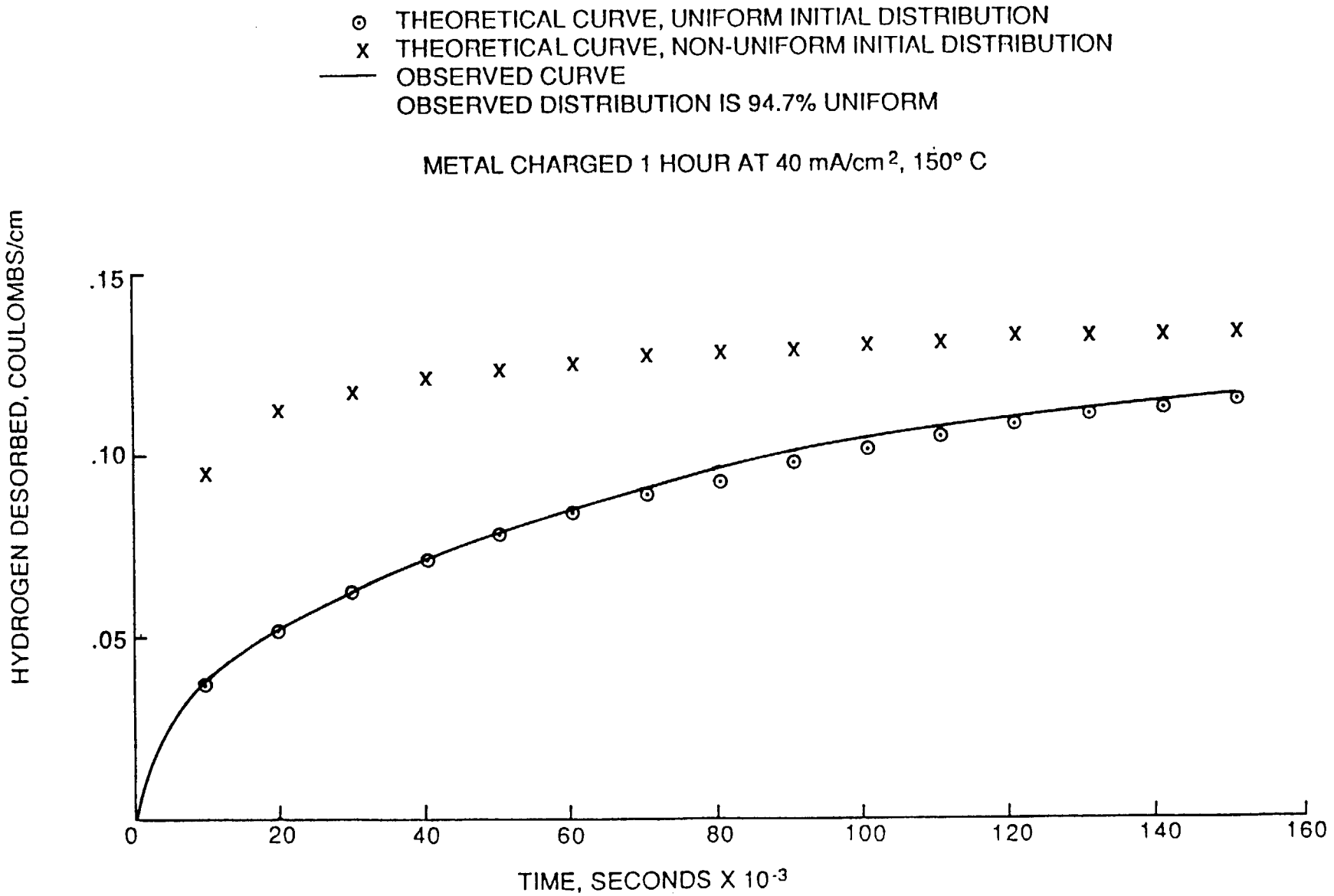

Figure 3. Hydrogen desorption curves for Inconel 718 cylinder charged at 150 °C.

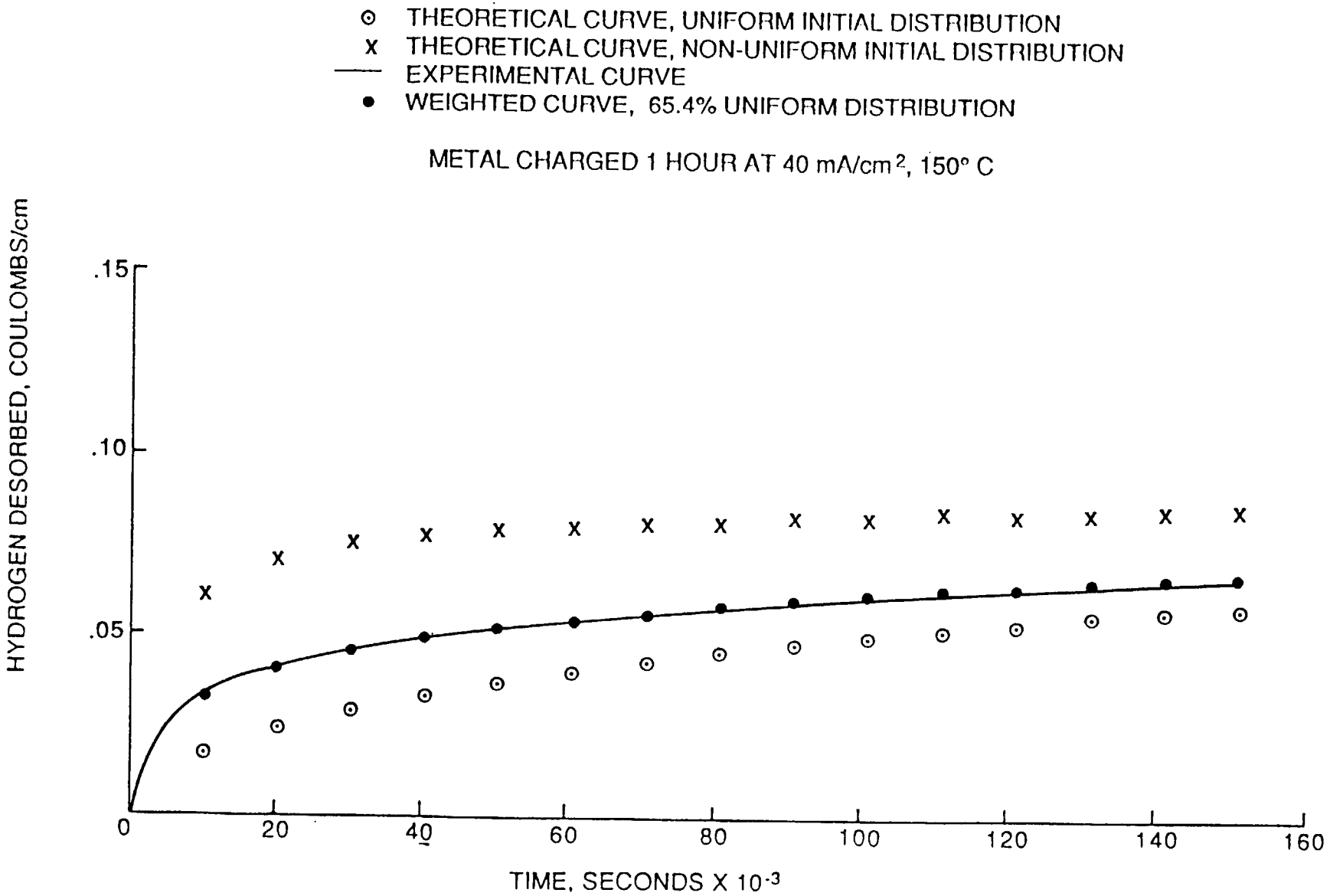

Figure 4. Hydrogen desorption curves for cold-worked Inconel 718 cylinder charged at 150 °C.

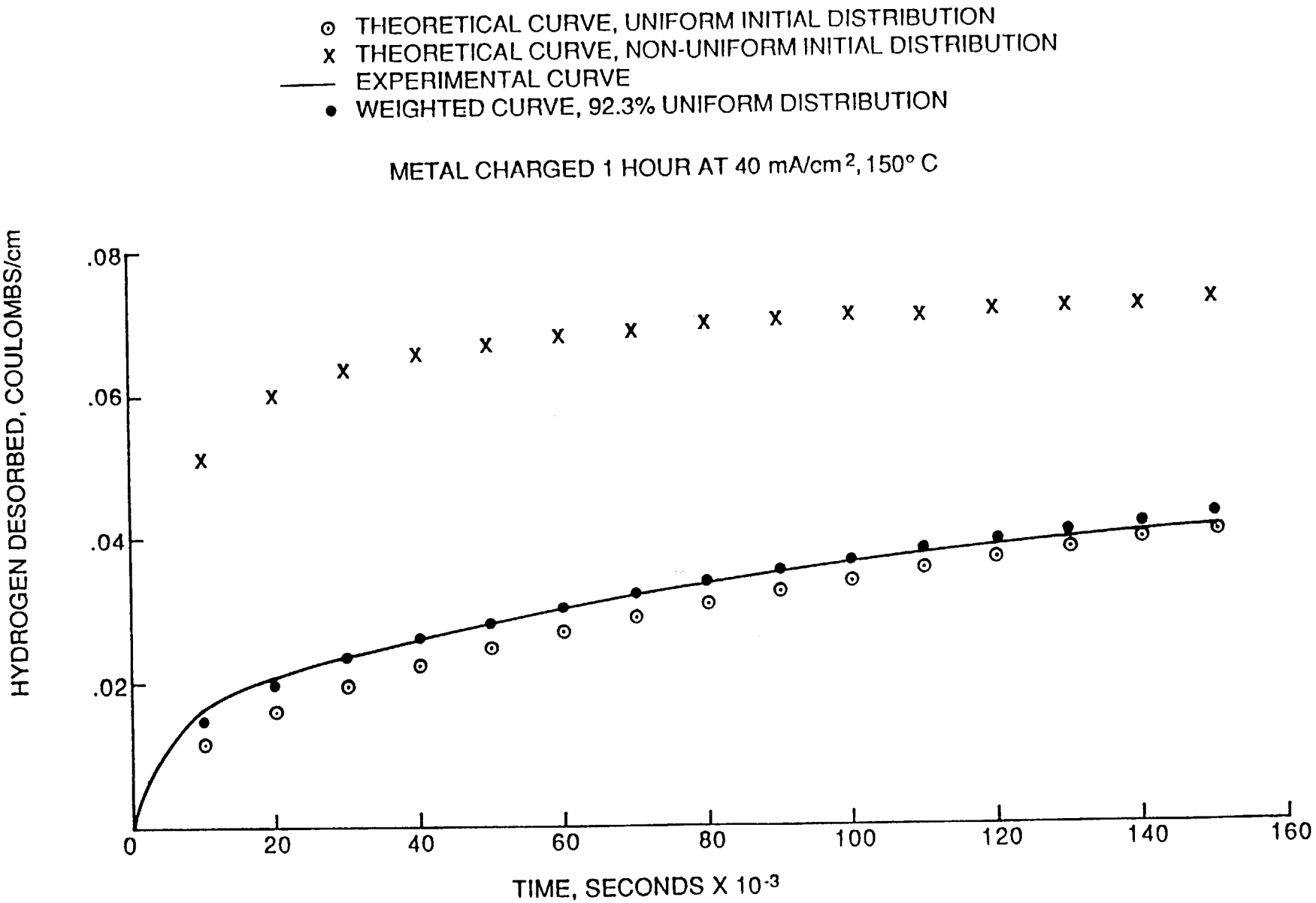

Figure 5. Hydrogen desorption curves for single crystal P&W 1480 cylinder charged at 150 °C.

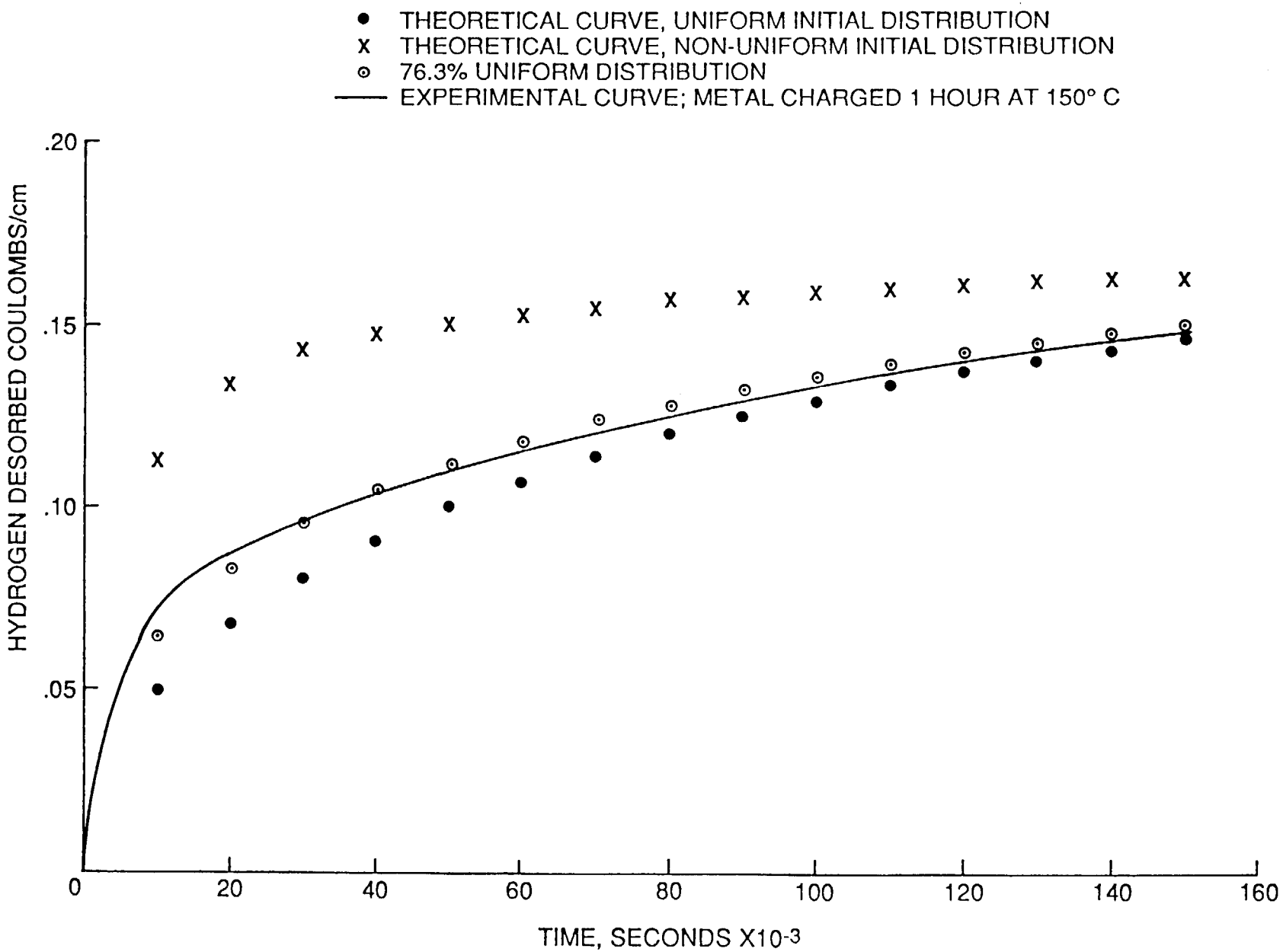

Figure 6. Hydrogen desorption curves for directionally solidified MAR-M-246 (Hf) cylinder charged at 150 °C.

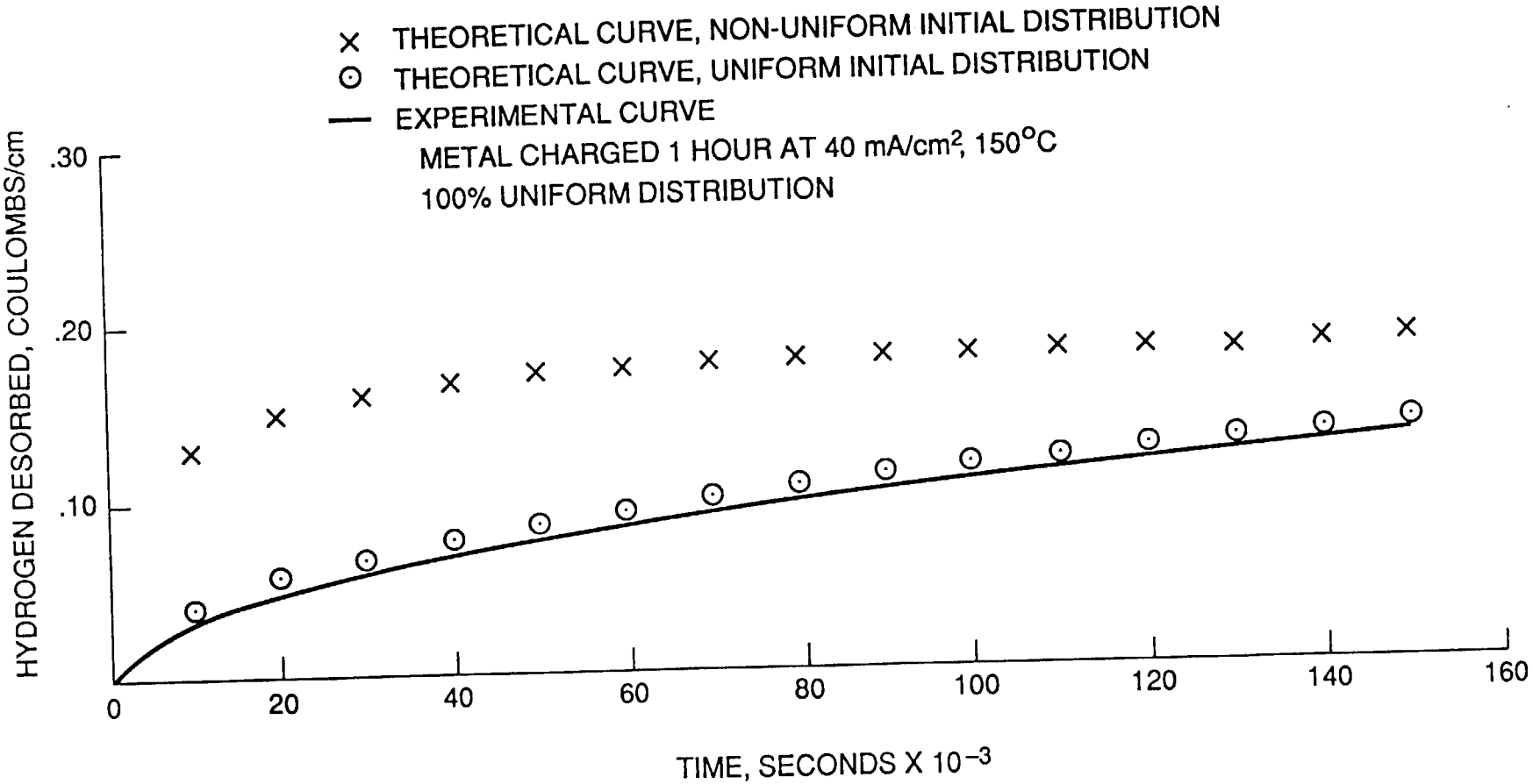

Figure 7. Hydrogen desorption curves for A-286 cylinder charged at 150 °C.

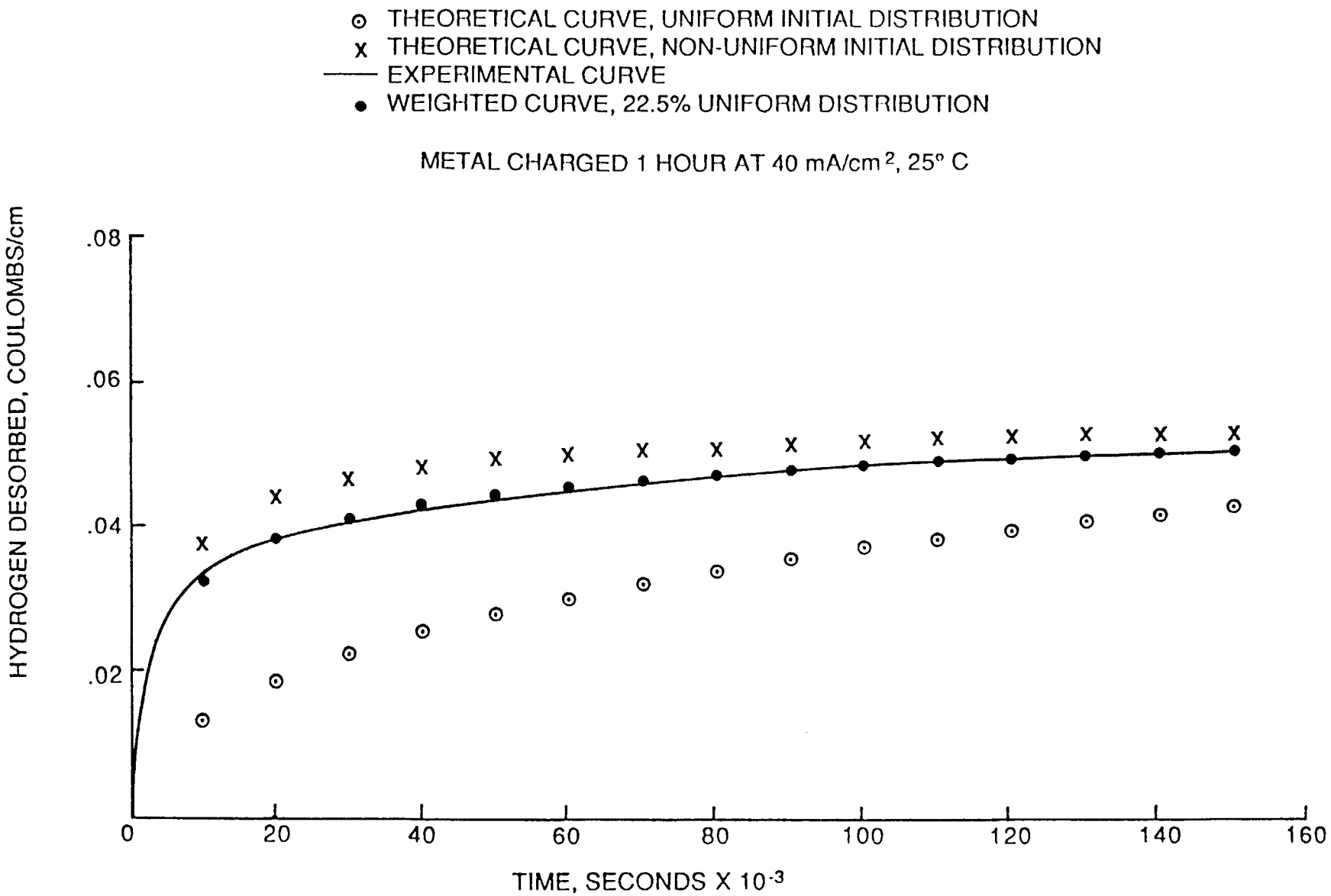

Figure 8. Hydrogen desorption curves for MP159 cylinder charged at 25 °C.

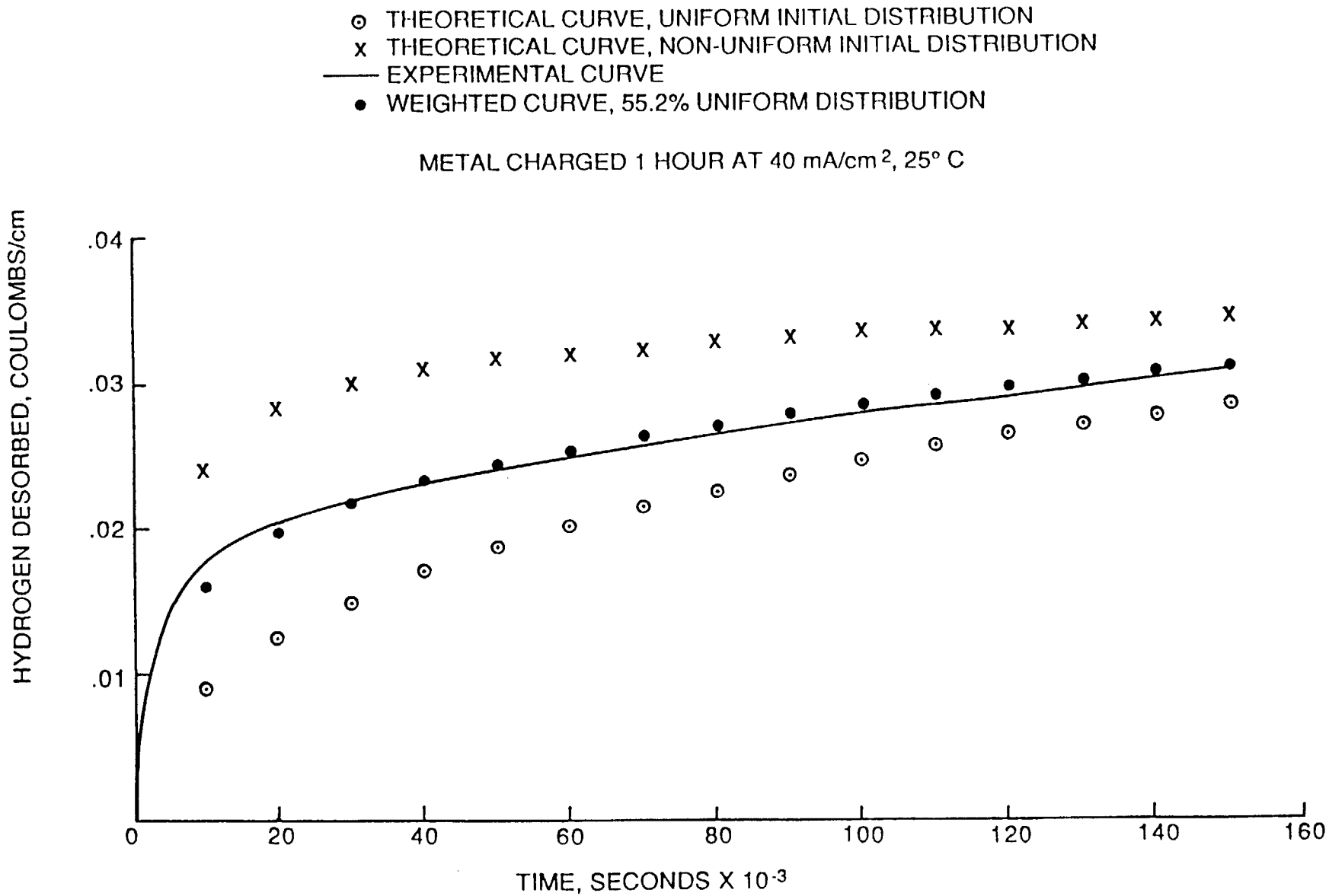

Figure 9. Hydrogen desorption curves for MP35N cylinder charged at 25 °C.

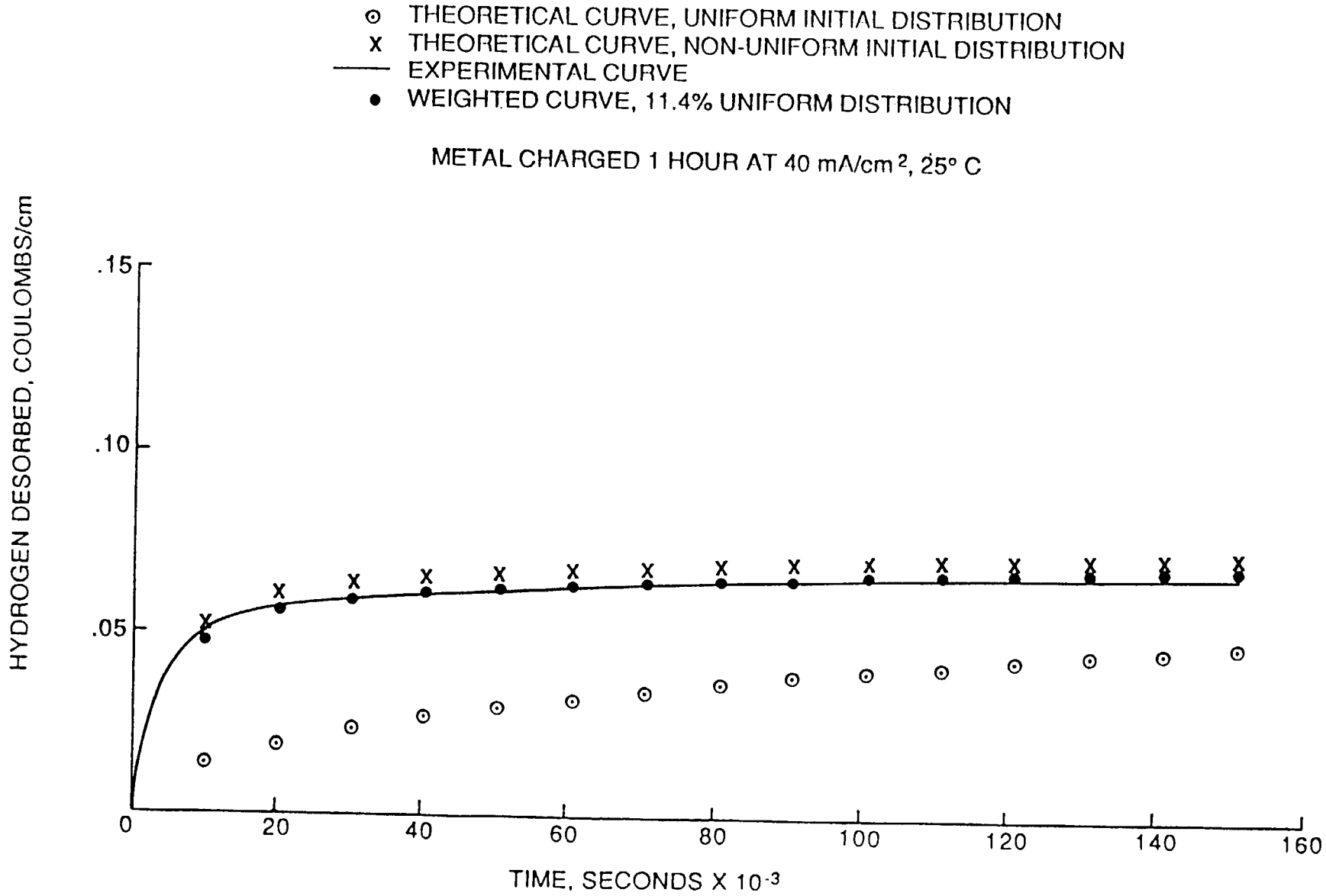

Figure 10. Hydrogen desorption curves for Inconel 718 cylinder charged at 25 °C.

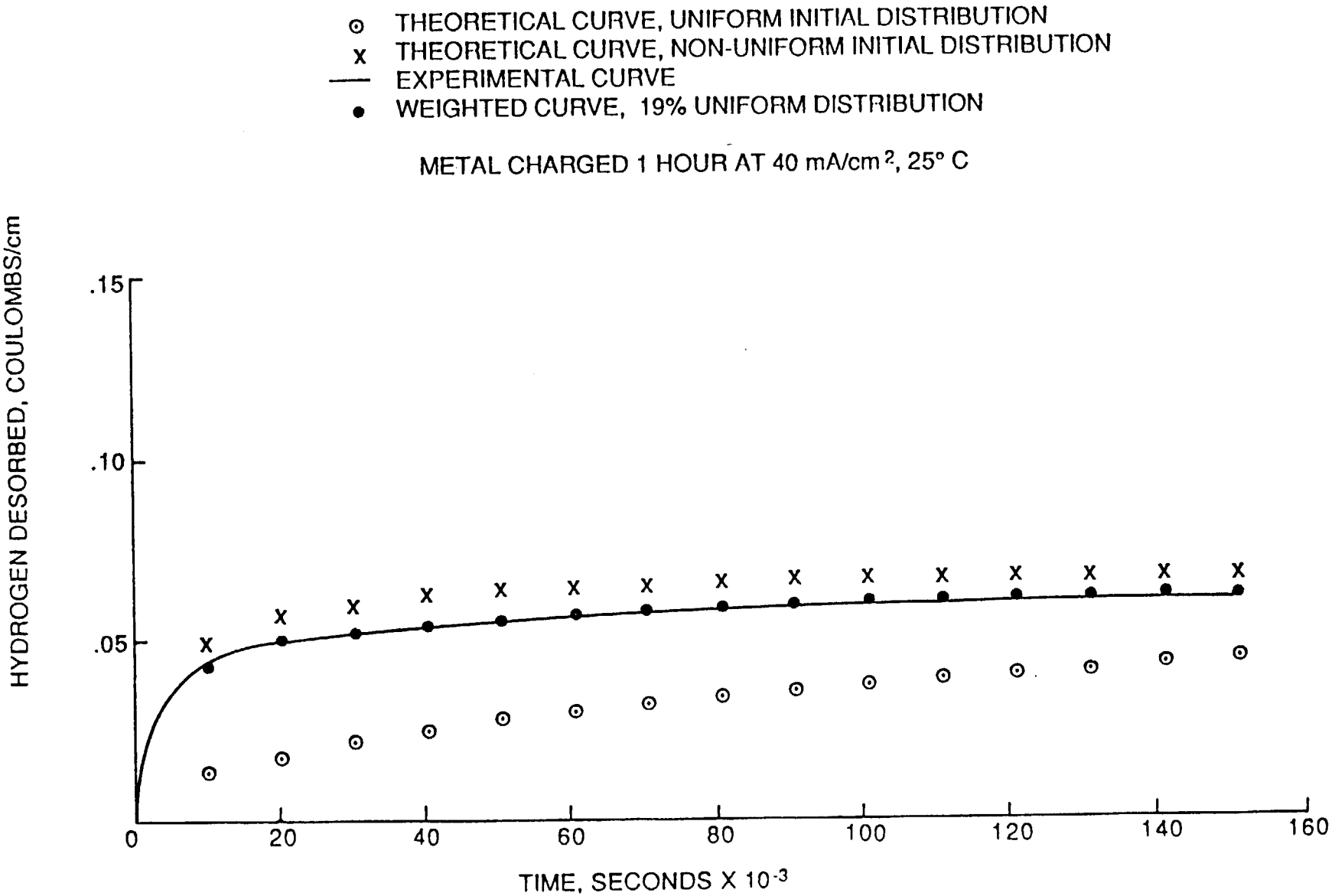

Figure 11. Hydrogen desorption curves for cold-worked Inconel 718 cylinder charged at 25 °C.

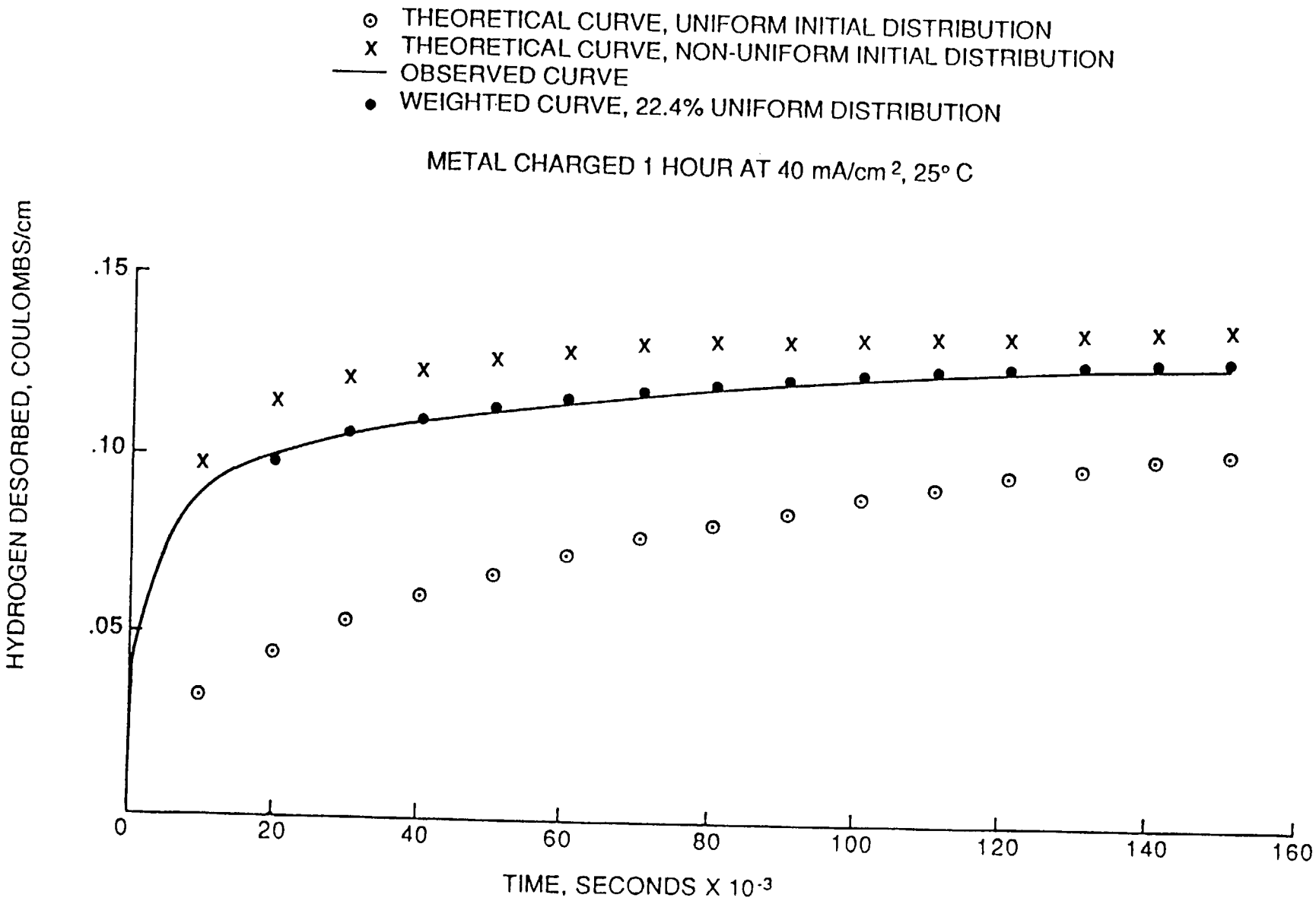

Figure 12. Hydrogen desorption curves for single crystal P&W 1480 cylinder charged at 25 °C.

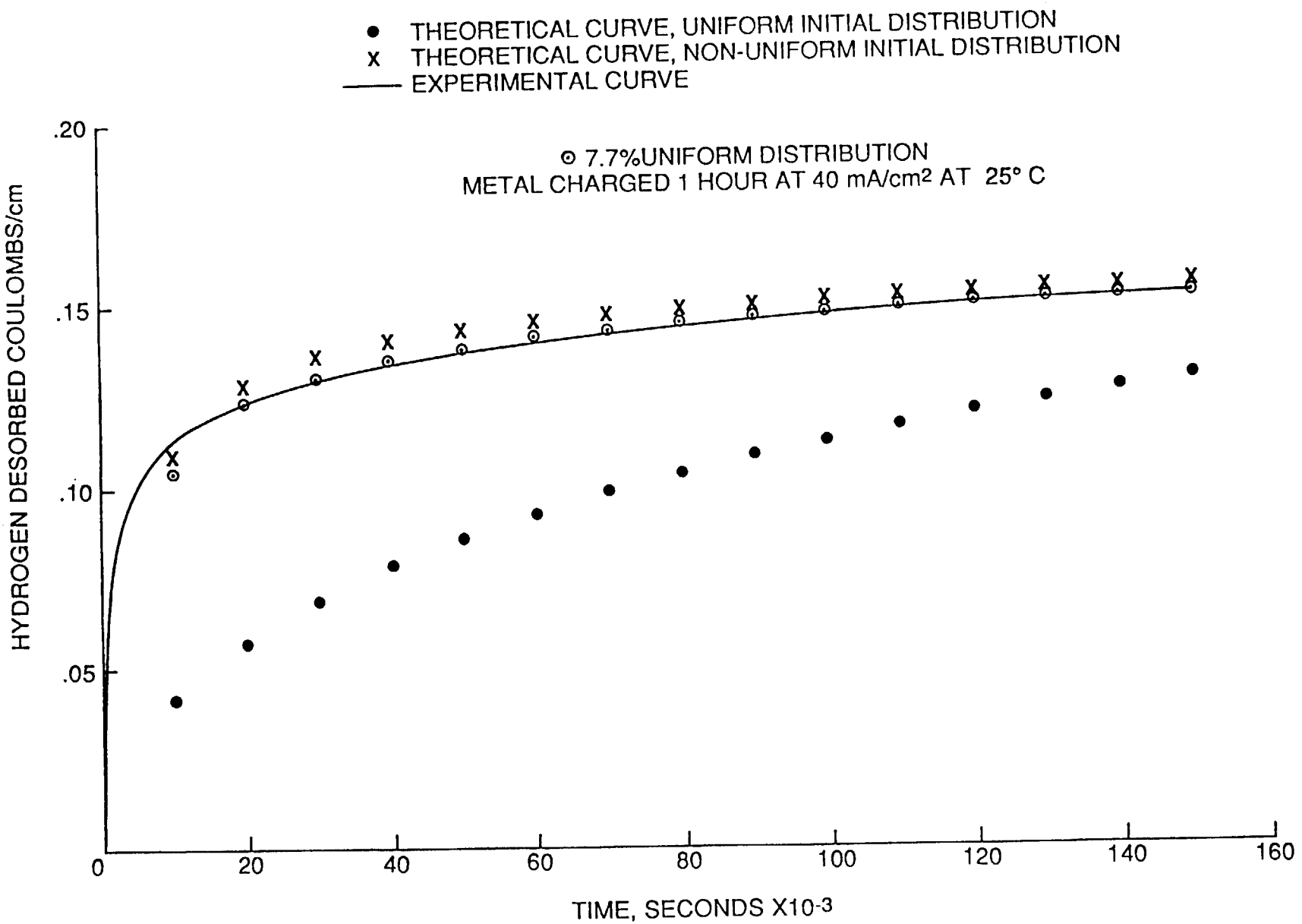

Figure 13. Hydrogen desorption curves for directionally solidified MAR-M-246 (Hf) cylinder charged at 25 °C.

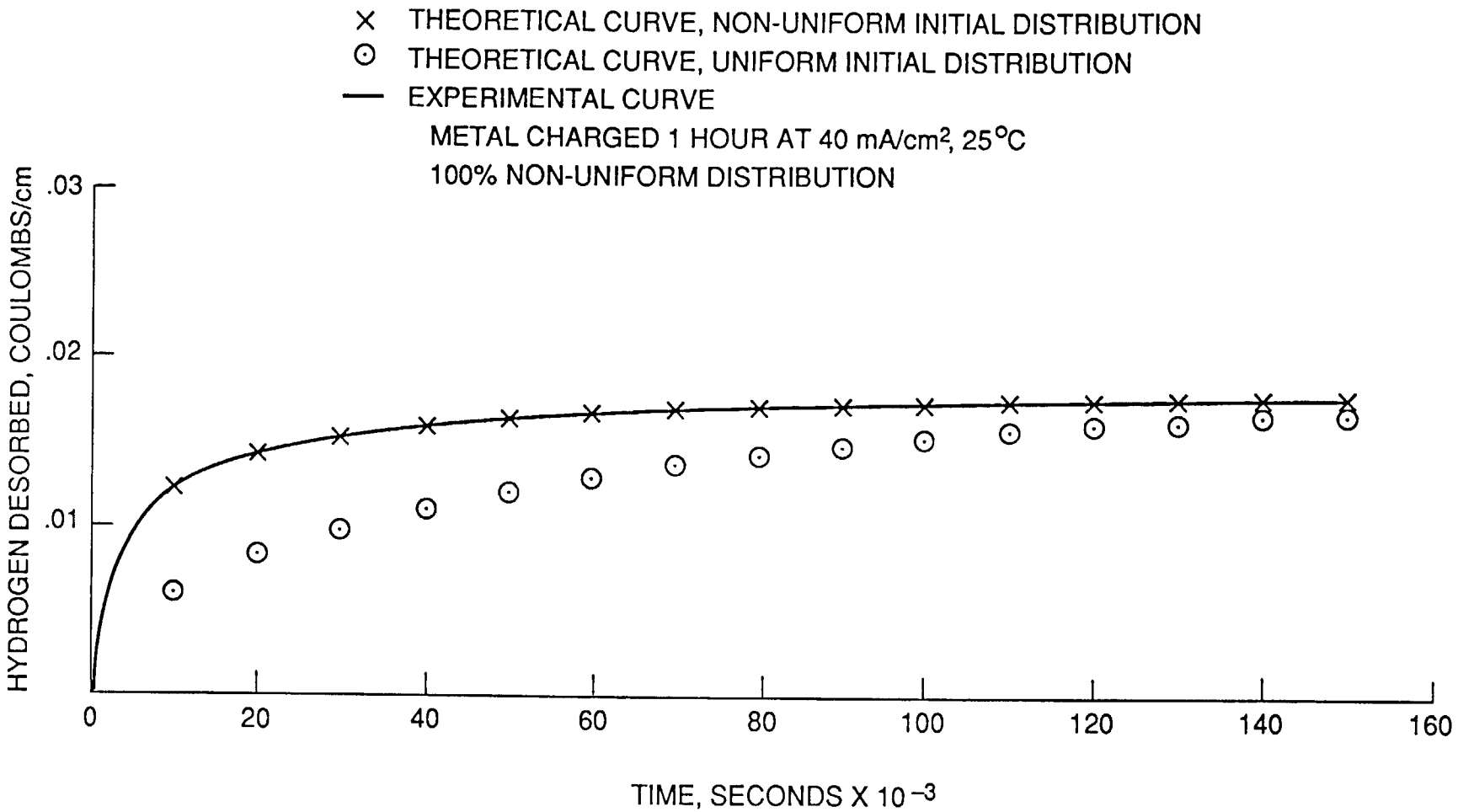

Figure 14. Hydrogen desorption curves for A-286 cylinder charged at 25 °C.

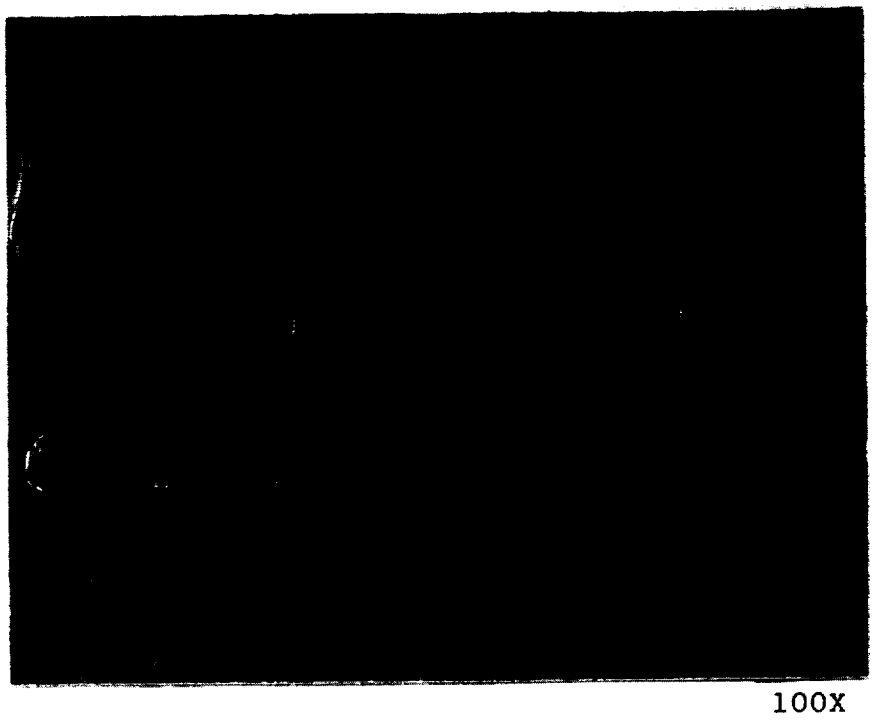

Figure 15. Grain structure in MP159.

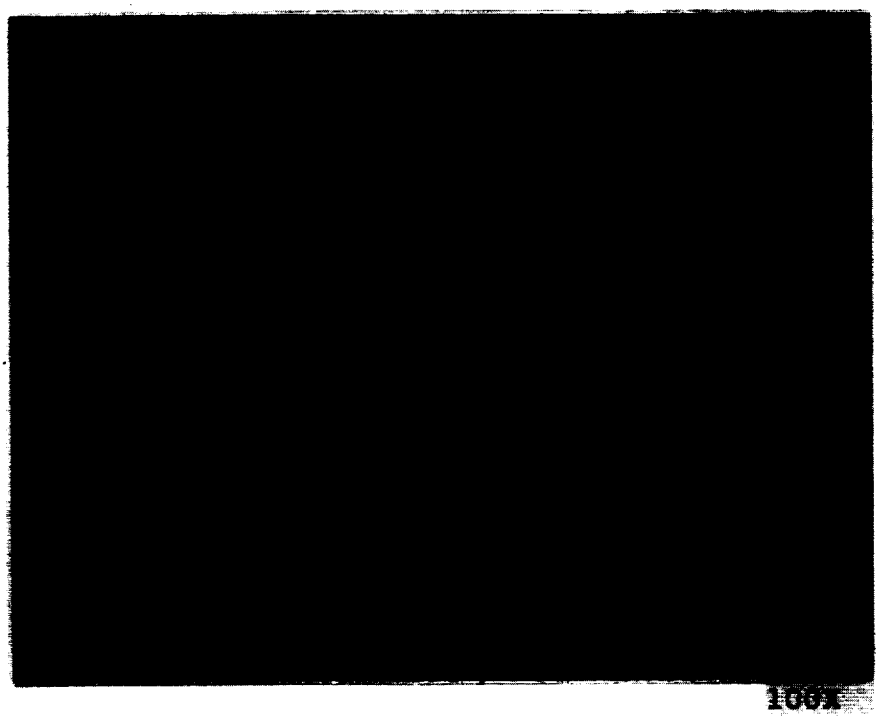

Figure 16. Grain structure in MP35N.

400X

Figure 17. Grain structure in Inconel 718.

400X

Figure 18. Grain structure in cold-worked Inconel 718.

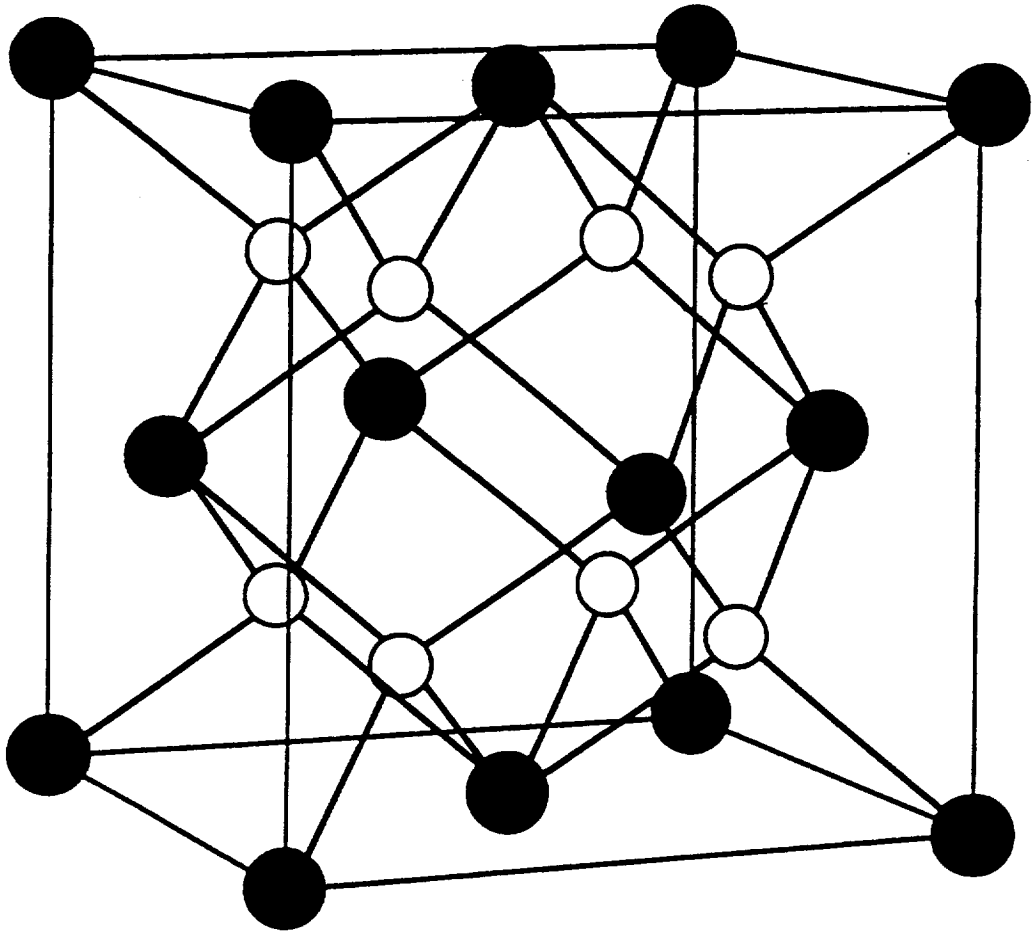

Figure 19. The fluorite structure.

NASA
National Aeronautics and Space Administration

Report Documentation Page

1. Report No.	2. Government Accession No.	3. Recipient's Catalog No.
NASA TP-3128		

4. Title and Subtitle	5. Report Date
The Interaction of Hydrogen With Metal Alloys	August 1991
	6. Performing Organization Code

7. Author(s)	8. Performing Organization Report No.
M.D. Danford and J.W. Montano	
	10. Work Unit No. M-664

9. Performing Organization Name and Address	11. Contract or Grant No.
George C. Marshall Space Flight Center Marshall Space Flight Center, Alabama 35812	
	13. Type of Report and Period Covered Technical Paper
12. Sponsoring Agency Name and Address	14. Sponsoring Agency Code
National Aeronautics and Space Administration Washington, DC 20546	

15. Supplementary Notes

Prepared by Materials and Processes Laboratory, Science and Engineering Directorate.

16. Abstract

Hydrogen diffusion coefficients have been measured for several alloys, and these have been determined to be about the same at 25 °C for all alloys investigated. The relation of structure, both metallurgical and crystallographic, to the observed hydrogen distribution on charging has been investigated, as well as the role of hydride formation in the hydrogen resistance of metal alloys. An attempt has been made to correlate the structures and compositions of metal alloys as well as other parameters with the ratios of their notched tensile strengths in hydrogen to that in helium, R(H_2/He), which are believed to represent a measure of their hydrogen resistance. Evidence supports the belief that hydrogen permeability and hydrogen resistance are increased by smaller grain sizes for a given alloy composition.

17. Key Words (Suggested by Author(s))	18. Distribution Statement
Hydrogen diffusion in metals Hydrides Hydrogen embrittlement Structure and hydrogen susceptibility	Unclassified-Unlimited Subject Category: 26

19. Security Classif. (of this report)	20. Security Classif. (of this page)	21. No. of pages	22. Price
Unclassified	Unclassified	36	A03

NASA FORM 1626 OCT 86

For sale by the National Technical Information Service, Springfield, VA 22161-2171

NASA-Langley, 1991